ACS NANO

www.acsnano.org

ARTICLE

In Situ Studies of Copper-Based CO_2 Reduction Electrocatalysts by Scanning Transmission Soft X-ray Microscopy

Chunyang Zhang, Haytham Eraky, Shunquan Tan, Adam Hitchcock, and Drew Higgins*

Cite This: *ACS Nano* 2023, 17, 21337−21348

Read Online

ACCESS | Metrics & More | Article Recommendations | Supporting Information

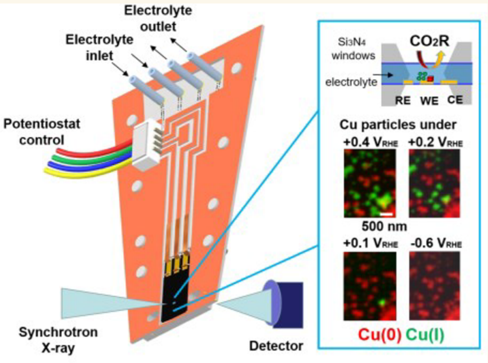

ABSTRACT: A microfluidic-enabled electrochemical device has been developed to investigate electrochemically active nanomaterials under reaction conditions using *in situ* scanning transmission soft X-ray microscopy (STXM). *In situ* STXM measurements were conducted on electrodeposited Cu catalysts under electrochemical CO_2 reduction (CO_2R) conditions. The study provides detailed, quantitative results about the changes in the morphology and chemical structure of the catalytic nanoparticles as a function of applied potentials. The deposited Cu nanoparticles initially contain both Cu(0) and Cu(I). As an increasingly cathodic potential is applied, the Cu(I) species gradually convert to Cu(0) over the potential range of +0.4 to 0 V versus the reversible hydrogen electrode (V_{RHE}). During this process, Cu(I) particles of various sizes are converted to metallic Cu at different reaction rates and at slightly different potentials, indicating a degree of heterogeneity in the electrochemical response of discrete particles. At CO_2R relevant potentials, only metallic Cu is observed, and the morphology of the particles is fairly stable within the spatial resolution limits of STXM (~40 nm). We also report *in situ* STXM studies of a working electrode with relatively thick Cu-based electrodeposits. The spatially resolved chemical analysis identifies that Cu-oxide species can persist under CO_2R conditions, but only when the catalytic nanoparticles are electronically isolated from the working electrode and therefore are catalytically irrelevant. In summary, *in situ* STXM is presented as a technique to gain advanced morphological and spatially resolved chemical structure insights into electrochemically active nanomaterials, which was used to provide improved understanding regarding Cu nanomaterial catalysts under CO_2 reduction conditions.

KEYWORDS: *electrochemistry, CO_2 reduction, in situ characterization, soft X-ray spectro-microscopy, electrocatalysis, electrocatalysts, scanning transmission X-ray microscopy*

1. INTRODUCTION

Carbon dioxide electroreduction (CO_2R) is a promising route to generate valuable fuels and chemical feedstocks through the electrochemical conversion of CO_2 into hydrocarbon, alcohol, and carbonyl products.[1−4] With electricity generated by renewable energy resources such as wind and solar, electrochemical CO_2 reduction has the potential to become a sustainable approach to produce carbon-based chemicals and fuels, which could replace conventional petrochemical processes, thereby reducing greenhouse gas emissions and helping to protect the global environment. Among the different catalysts studied, copper (Cu) is the only known element that can convert CO_2 into valuable multicarbon products (C_{2+}) in appreciable quantities.[5−7] Unfortunately, despite much progress in recent years, the poor conversion efficiency, limited control of product distribution, and low stability of Cu-based electrocatalysts limit large-scale application of CO_2R.[8,9]

Improved understanding of Cu catalysts during electrochemical CO_2R is crucial for the development of high-performance, selective, and practical electrocatalysts, yet there remains debate over the nature of active site structure(s) and their evolution under reaction conditions. For example, the presence of oxidized Cu (Cu(I) and/or Cu(II) species) or subsurface oxygen during electro-reduction has been suggested to improve CO_2R activity and steer the selectivity toward C_{2+} products such as ethanol and ethene.[10−12] However, other

Received: June 30, 2023
Revised: October 23, 2023
Accepted: October 25, 2023
Published: October 31, 2023

https://doi.org/10.1021/acsnano.3c05964
ACS Nano 2023, 17, 21337−21348

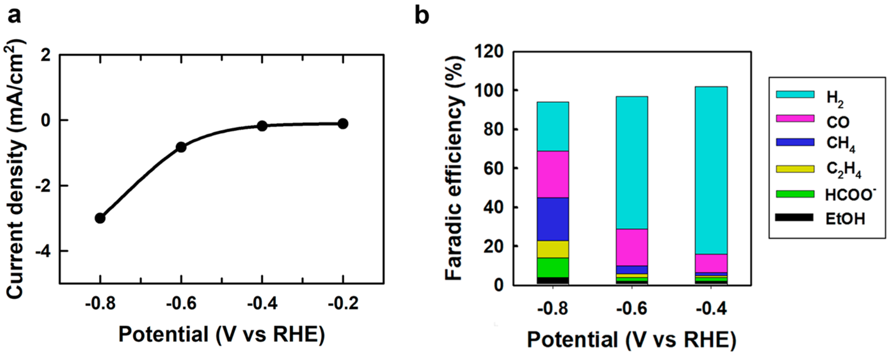

Figure 1. Evaluation of activity and selectivity for electrochemical CO_2 reduction by electrodeposited Cu catalysts in CO_2-saturated 0.1 M $KHCO_3$ in a custom-built two-compartment membrane separated cell. (a) Overall geometric current density. (b) Faradaic efficiency toward various products under −0.4, −0.6, and −0.8 V_{RHE}.

studies have refuted the presence of non-zero-valent Cu species under the electrochemically reducing conditions required for the reaction.[13−15] Morphological changes of Cu electrocatalysts during the CO_2R process have also been demonstrated, leading to rapid restructuring of catalytic structures, which correlate with observed changes in activity and selectivity.[16,17] Overall, the morphology and chemical structures present in Cu catalysts change as a direct function of the local reaction environment and applied potential, which draws into question the suitability of using *ex situ* characterization techniques to study Cu-catalyzed CO_2R processes. This has motivated the development and application of *in situ/operando* spectroscopy, microscopy, and spectro-microscopy techniques to provide real-time and same-position characterization of working catalysts under electrochemical reaction conditions.[18−21] *In situ* transmission electron microscopy (TEM) has been used as a method for studying CO_2R electrocatalysts due to its excellent spatial resolution on the order of a few to tens of nanometers that enables imaging of the morphology of an electrocatalyst and how it evolves under reaction conditions.[16,17,22−25] *In situ* TEM has also been coupled with selected area electron diffraction to identify crystalline phase structures present under reaction conditions.[16,17,22,23] While TEM instruments are commonly equipped with core level electron energy loss spectroscopy (EELS) capabilities that can provide spatially resolved chemical speciation, conducting EELS under *in situ* electrocatalysis conditions is challenging due to strong electron−liquid interactions that lead to spectral distortion. This challenge provides the opportunity for the development and implementation of alternative techniques that can simultaneously provide spatially resolved imaging of the morphology and chemical structures present in materials under reaction conditions.

In this work, we have used *in situ* soft X-ray scanning transmission X-ray microscopy (STXM)[26−35] to characterize Cu electrocatalysts in a microchip electrochemical cell designed to achieve electrolyte flow under applied electrochemical potentials which closely resemble the conditions experienced by Cu particles in a laboratory-scale CO_2R reactor. STXM is a synchrotron-based spectro-microscopic technique that can simultaneously provide microscopic imaging of catalyst morphologies alongside spatially resolved (∼40 nm spatial resolution)[36,37] spectroscopic characterization through near-edge X-ray absorption fine structure (NEXAFS) spectroscopy[36] to enable quantitative, chemically selective imaging. This can overcome some of the limitations of techniques such as *in situ* diffraction[38] or *in situ* X-ray absorption spectroscopy[39−41] that provide only bulk-averaged characterization and no morphological insight. It can also complement *in situ* electron microscopy,[16,17,22−25,42,43] which provides region-specific morphological characterization at extremely high spatial resolution but limited insight into local chemical structures owing to the difficulty of performing high-resolution electron energy loss spectroscopy in the presence of a liquid electrolyte.

By utilizing a microfluidic-based flow electrochemical microchip reactor, *in situ* STXM was used to characterize the morphology and chemical structure(s) present in electrodeposited Cu nanoparticle catalysts under electrochemical CO_2 reduction conditions as a function of time and electrode potential. The microfluidic-based electrochemical device enabled controlled electrolyte flow and could achieve an aqueous electrolyte thickness of <2 μm[34,35] to enable soft X-ray transmission-mode measurements. *In situ* STXM measurements provided a detailed quantitative evaluation of particle evolution as a function of local chemical environments and applied potential. In this study the electrodeposited Cu particles are initially composed largely of Cu(I) species that convert to metallic Cu (denoted as Cu metal or Cu(0)) at potentials ∼0.2 V more positive than the onset of CO_2R. Significant changes in the particle morphology accompany the reduction of Cu-oxide species into metallic Cu. We also identify conditions where Cu-oxide species persist under reducing electrochemical CO_2R conditions and find that this is an artifact due to electronic isolation of the Cu particles from the working electrode when thick electrodeposits are used. We find no evidence of kinetically or diffusion-trapped Cu-oxide species in catalytically relevant particles with electronic connectivity to the electrode. Overall, *in situ* STXM has enabled spectro-microscopic insight into the behavior of Cu catalysts under CO_2R conditions. The techniques reported here can be readily translated to other electrochemical materials/processes to gain insight into the morphology and spatially resolved chemical structures present in electrochemically active materials.

2. RESULTS

2.1. Electrochemical CO_2 Reduction Evaluation. The catalytic performance of electrodeposited Cu nanoparticles for CO_2 reduction in CO_2-saturated 0.1 M $KHCO_3$ was evaluated in a custom-built two-compartment electrolyte membrane separated cell that has been reported previously[44,45] (Figure S-1a), with results displayed in Figure 1. Details for catalyst electrode synthesis, experimental details, catalytic efficiency, and product distribution measurements are presented in Section 5.1. At an electrode potential of −0.4 V_{RHE}, the deposited Cu sample showed a current density of −0.18 mA/cm^2 (Figure 1a) with the majority of current going toward the production of H_2 with a Faradaic efficiency of 86% (Figure 1b). Small amounts of other products (CO, hydrocarbons, and alcohols) were detected, suggesting that CO_2R reactions have started to occur but with slow kinetics at this electrode potential. When the potential reached −0.6 V_{RHE}, the overall current density increased to −0.83 mA/cm^2 and there was a larger amount of CO_2R products (29% Faradaic efficiency) compared with that at −0.4 V_{RHE}. At −0.8 V_{RHE}, the formation of CO_2R products dominated and the Faradaic efficiency for H_2 production was only 25%. This shows that the CO_2R reactions started to increase the overall reaction rate from −0.6 V_{RHE} and became the main electrochemical reactions at more negative potentials. In general, electrochemical CO_2R on Cu does not occur at appreciable rates at potentials more positive than ca. −0.65 V_{RHE}.[44] In this case, it is important to note that the Cu particles were electrodeposited on Au, a well-known CO_2 to CO catalyst, to mimic the electrode configuration used for *in situ* STXM measurements. It is the presence of Au that likely underlies the CO_2R products formed, as Au can produce CO electrochemically, which can either be released as a product or be subsequently reduced to alcohols and carbonyls by Cu at potentials as positive as −0.4 V_{RHE}[46] via a tandem catalytic reaction scheme.[47,48]

2.2. *In Situ* STXM Experiments in a Microfluidic Electrochemical *in Situ* Device.

All *in situ* STXM experiments were conducted using a custom-built microfluidic electrochemical *in situ* device, which differs in several significant ways from existing commercial electrochemical liquid devices (Figure 2a; the details are discussed in Section 5.2)[34,35] This *in situ* microfluidic device is a major improvement compared to our previously reported 3D-printed device.[30] It is more reliable with respect to electrolyte handling and can provide an electrolyte layer thickness of ~1.6 μm with a continuous flow of 25 μL/h, which provides good ionic conductivity while being thin enough for STXM studies at the Cu 2p edge (Section S-5, Figure S-5). A relatively low flow rate (25 μL/h) was used to avoid bulging of the SiNx window, which would result in increased electrolyte thickness. The 25 μL/h flow rate is such that the electrolyte in the electrochemically active area of the *in situ* cell is changed every ~0.05 s. The two inlet and two outlet flow channels facilitate changing the electrolyte in minutes (rather than hours when using single inlet/outlets)[30] and are very useful for reducing the inner pressure and removing air or gaseous product bubbles. The light weight of the device, due to the fabrication of components using plastic and polymers rather than steel, improves the stability and reduces vibration in STXMs when the sample is scanned. The *in situ* microchip design includes a working electrode (WE), reference electrode (RE), and counter electrode (CE) that are all observable and measurable within the silicon nitride window area (Figure 2b,c), as opposed to many *in situ* electrochemical microchip designs that only provide visibility of the working electrode. Imaging all three electrodes is useful for being able to track unexpected electrochemical phenomena and to gain a holistic picture of all electrochemical processes occurring within the system. In this

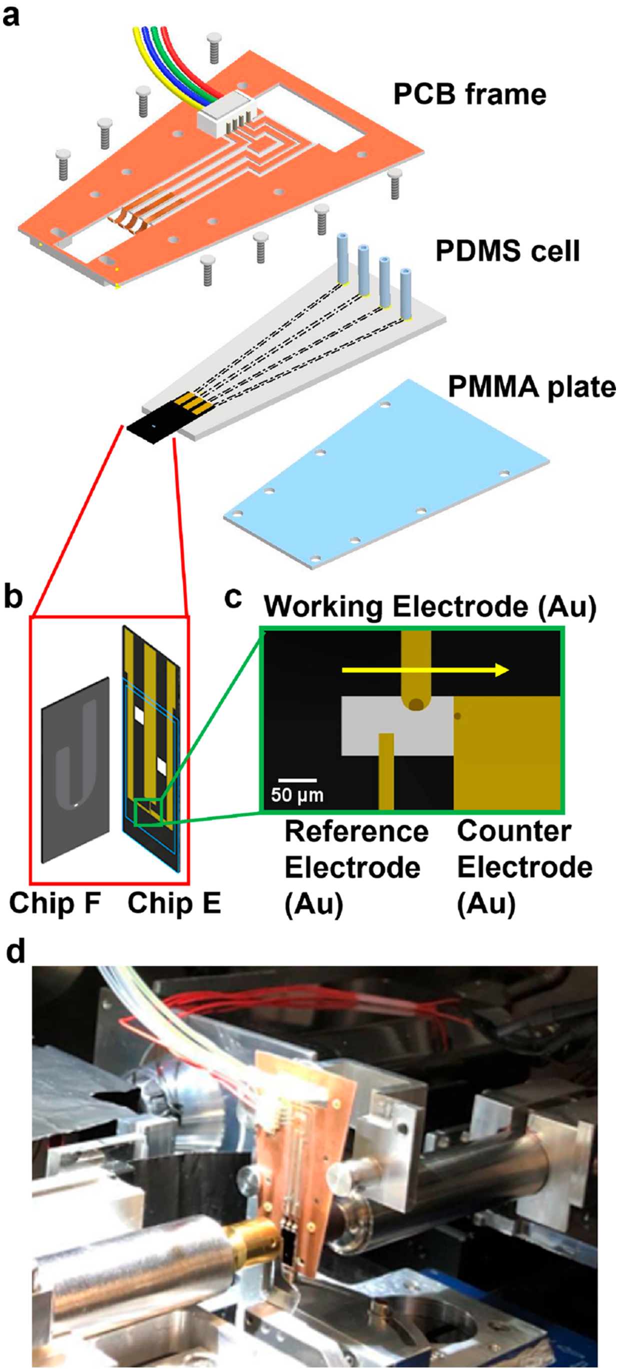

Figure 2. Microfluidic-based flow electrochemical device for *in situ* STXM experiments. Schematics describing (a) the *in situ* device consisting of three parts: a machined printed circuit board (PCB), a polydimethylsiloxane (PDMS)/glass microfluidic cell equipped with the electrochemical *in situ* chips (PDMS cell), and a poly(methyl methacrylate) backplate (PMMA plate) and (b) *in situ* chips consisting of two parts: base chip E containing three micro-Au-electrodes and spacer chip F with a predeposited 1 μm spacer defining the height of the electrolyte flow channel within the microchip setup. (c) Three-micro-Au-electrodes region on base chip E. The Si_3N_4 window area is 240 μm wide and 100 μm high. The thicknesses of the Si_3N_4 windows are 100 nm (base chip E) and 50 nm (spacer chip F). The areas used for STXM studies (dark circles on working and counter electrodes) are 20 μm in diameter and have a coating consisting of 5 nm Cr and 15 nm Au. The arrow indicates the direction of electrolyte flow. (d) Photo of the device inside the CLS ambient STXM.

study the electrolyte flow was from the WE to the CE. Figure 2d is a picture of the device inside the ambient STXM microscope at the Canadian Light Source (CLS) spectro-microscopy beamline, 10ID-1.

To ensure the local chemical environment present at the surface of the working electrode in our *in situ* device closely mimics the conditions at the working electrode of the two-compartment membrane separated cell used for CO_2R activity/selectivity evaluation, cyclic voltammetry (CV) of electrodeposited Cu particles in the two-compartment cell was collected and compared with the CV of electrodeposited Cu (prepared using the same methods) from the *in situ* device (Figure S-1). Qualitatively, the CV behavior was the same for the two cells, indicating a similar electrochemical reaction environment. Quantitatively the currents from the microchip electrode cell were several orders of magnitude lower, which is due to the reduced dimensions (geometric electrode area of ~2200 μm^2 in the *in situ* cell versus 5.7 cm^2 in the reactor), but the current density was in fact higher (see Figure S-1f). Ultimately, the measurements reported here demonstrate that the electrodeposited Cu catalysts have a very similar electrochemical response and thus local reaction environments in our *in situ* STXM microchip reactor as that in the two-compartment cell used for CO_2R activity/selectivity evaluation. This ensures that the morphological changes and chemical states (oxidation states) observed and mapped by STXM spectro-microscopy are catalytically relevant.

2.3. *In Situ* STXM of Electrodeposited Cu Particles. Cu particles were electrodeposited from a 5 mM $CuSO_4$/KCl solution onto the Au working electrode of the custom-designed *in situ* STXM device using multiple CV scans as described in Section 5.4. The deposition of Cu-based particles was confirmed by measuring STXM transmission images at 933.5 eV, the peak Cu 2p X-ray absorption energy for both Cu(I) and Cu(0) species. As shown in Figure 3a, the electrodeposited Cu typically consisted of particles ranging in size from tens of nanometers to ~0.8 μm, distributed across the Au-coated working electrode. After Cu particle deposition, a four-energy (4-E) Cu 2p STXM stack was recorded at a region showing well-defined Cu particles (see inset of Figure 3a) to identify the composition of the electrodeposited Cu particles. This STXM stack measurement probes the catalyst at four specific photon energies which were carefully chosen to directly identify and map the oxidation states present in the Cu-based particles while enabling significantly accelerated measurements versus recording a stack measurement at closely spaced energy values across the Cu 2p edge. The stack was fit using the reference spectra of Cu(0) and Cu(I) (Figure 3b) to generate component maps for each species (Figure 3c,d, Figure S-7). The component maps were then combined, using rescaling within each color, to generate color-coded component maps such as the one shown in Figure 3e. The intensity scales in Figure 3c and d indicate the thickness in nanometers of the indicated species. To verify the analyses, spectra of the Cu(0) and Cu(I) regions were extracted and compared with reference spectra (Figure S-8). The extracted spectra from Cu(0) and Cu(I) regions correctly showed that each species was the dominant component.

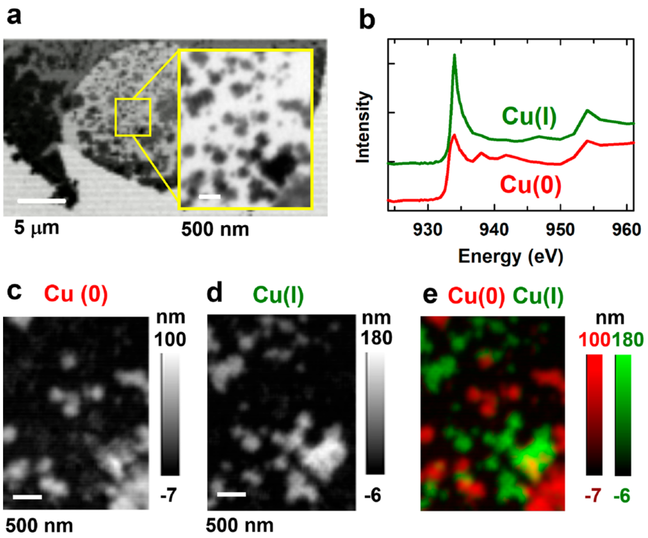

Figure 3. Illustration of STXM investigation of *in situ* electrodeposited copper particles. (a) Transmission image at 933.5 eV. (b) Cu 2p X-ray absorption spectra of Cu(0) (Cu metal) and Cu(I) from Cu_2O. Quantitative component maps of (c) Cu(0) and (d) Cu(I) derived from fitting reference spectra to a 4-E stack. (e) Color-coded composite (rescaled) of the Cu(0) (red) and Cu(I) (green) maps.

2.4. Quantitative *in Situ* STXM on Cu Particles during CO_2R. After electrodeposition of the Cu particles, the electrolyte was changed from 5 mM $CuSO_4$/KCl to CO_2-saturated 0.1 M $KHCO_3$ (Section 5.5). Chronoamperometry holds at various potentials (+0.4, + 0.2, +0.1, 0, −0.1, −0.2, −0.4, −0.6 V_{RHE}) were applied in sequence, with a 30 s hold at +0.4 V_{RHE} applied between each new electrode potential to ensure the catalyst was in the same starting state. Figure 4a plots the current density obtained from chronoamperometry as a function of applied potential during the *in situ* STXM measurements. Figure 4b depicts the electrode potential profile used throughout the process. At each applied potential, two STXM images (image 1 and 2 at 933.5 eV, ~3 min for each), a fast four-energy STXM stack scan (4-E stack, 920, 933.5, 937, and 960 eV, ~7 min) and a complete Cu 2p STXM stack scan (full stack, 53 energies from 920 to 965 eV, ~30 min) were conducted. Collecting two STXM images, one at the start of the measurements and one at the end, enabled us to track the morphological changes that occurred over the course of the measurements. The results from the 4-E stack and the full stack showed the evolution of the morphology and oxidation state of the Cu particles on different time scales, with the 4-E stack covering the first ~3−10 min of the measurements and the full stack covering ~10−40 min after the specified electrode potential was applied.

Figure 5 presents the results collected on the Cu particles under CO_2R conditions following this protocol. It includes STXM images 1 and 2 alongside color-coded composite maps of the Cu(0) and Cu(I) species obtained from analysis of the 4-E and the full stacks at potentials ranging from +0.4 to −0.6 V_{RHE}. The complete STXM results are presented in Section S-8, Figure S-9. The morphology and oxidation states of the Cu particles were observed during different time periods (0−3, 3−10, 10−40, 40−43 min) under various potentials. From +0.4 to +0.2 V_{RHE}, the Cu(I) particles decreased in size by an extent proportional to their original size. It is easiest to observe the changes of large Cu(I) particles in region A1 (outlined by a blue square on the 4-E color-coded map at +0.4 V_{RHE}). The particles in this region were interconnected at +0.4 V_{RHE}, but at +0.2 V_{RHE} became smaller in size and more discrete from the Cu agglomerates. For the very small Cu(I) particles outside

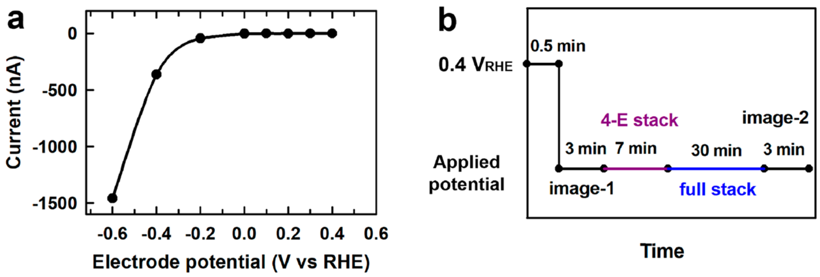

Figure 4. *In situ* STXM studies of Cu particles as a function of potential. (a) Average current at various potentials during chronoamperometric measurements in the *in situ* device. (b) Illustration diagram to show the STXM measurements at each applied potential.

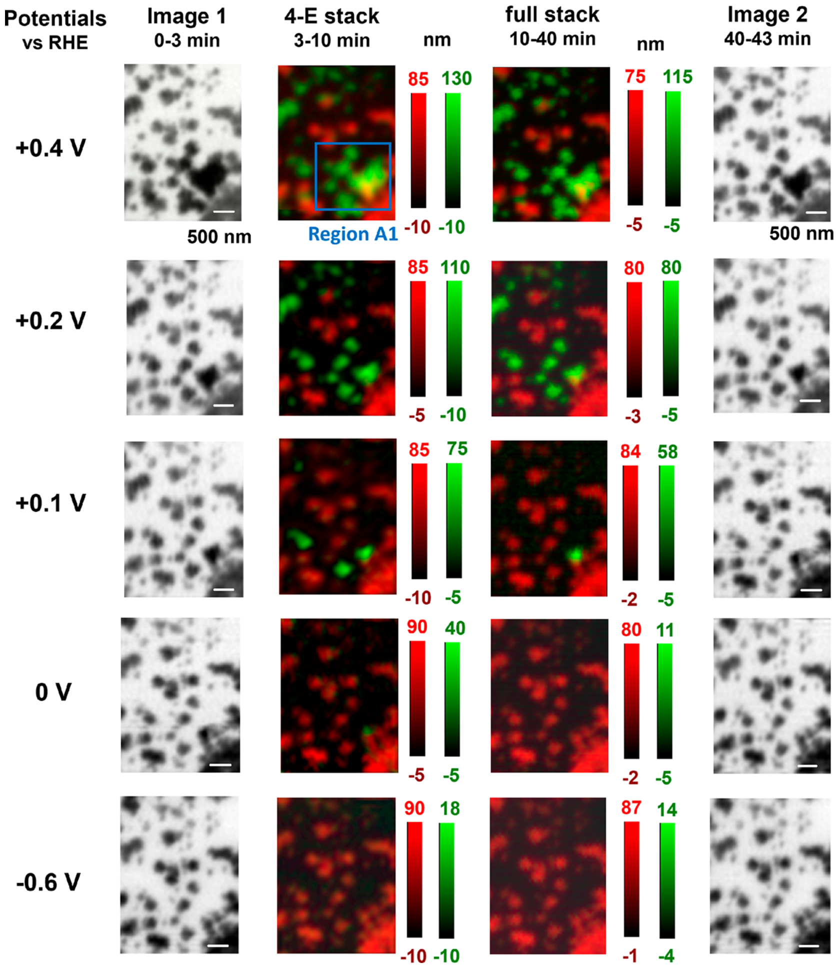

Figure 5. Evolution of Cu particle morphology and chemistry with decreasing potential. (Left 1) Image 1 at 0−3 min under applied potentials. (Left 2) Color-coded composites of Cu(0) (red) and Cu(I) (green) maps at the indicated potentials (vs RHE) derived from four-energy stacks (3−10 min). (Right 2) Color-coded composites of Cu(0) (red) and Cu(I) (green) maps at the indicated potentials (vs RHE) derived from 54-energy full stacks (10−40 min). (Right 1) Image 1 at 40−43 min under applied potentials. The dwell time for all *in situ* STXM measurements was 3 ms/pixel.

region A1, it was hard to observe size reduction due to the limited spatial resolution. Furthermore, no apparent particle size reduction occurred at the Cu(0) particles. Similar structural shrinking of Cu(I) particles has been reported by other researchers,[49] most likely arising due to the structural contraction from removal of the oxygen atoms in Cu-oxide. Moreover, from +0.4 to +0.2 V_{RHE}, the amount of Cu(I) present in the particles was reduced to a certain extent. After applying a more reducing potential of +0.1 V_{RHE}, conversion of most of the Cu(I) to metallic Cu(0) was observed, with Cu(I) species found to reduce over a time scale of minutes, as seen by comparing the slightly higher portion of Cu(I) particles present in the 4-E stack (collected over the first 3−10 min of measurement) versus the full stack measurement (collected over the first 10−40 min of measurement). These results show that not all of the Cu(I) species convert to metallic Cu at the same time, despite the fact that all particles are nominally experiencing the same applied electrode potential. The Cu(I) species that remained at +0.1 V_{RHE} continued to decrease in size when the electrode potential was reduced to 0 V_{RHE}. No

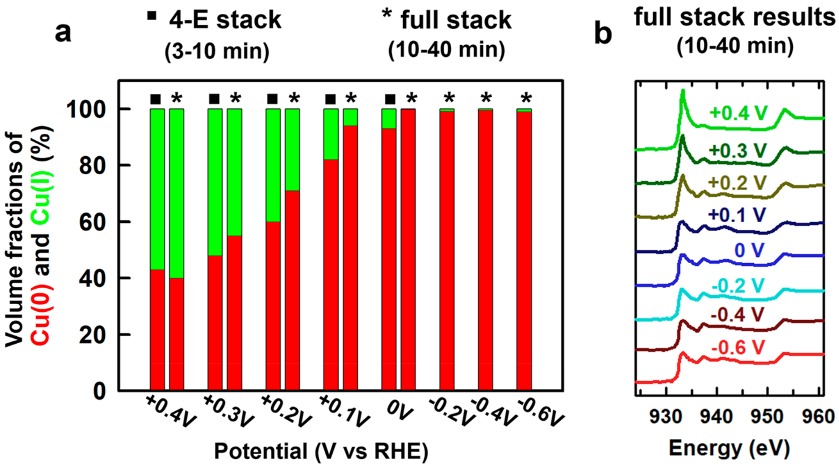

Figure 6. Quantitative analysis of composition from Cu 2p spectroscopy. (a) Percentage volume composition of Cu(I) and Cu(0). (b) Average spectra of the particles from the 53-energy full stacks at various potentials.

Cu-oxide species were observed after several minutes at this electrode potential. Ultimately, these results demonstrate that the reduction of Cu(I) happens at various times and electrode potentials for different particles, but at electrode potentials from 0 to −0.6 V_{RHE}, only Cu(0) species remain. In addition, after complete reduction to Cu(0) species, the Cu particles largely maintained the same morphology during ~43 min of chronoamperometry (CA) at −0.6 V_{RHE} under CO_2R conditions. Due to the use of OD1 reference spectra (Figure 3b), the absolute thickness of the Cu(0) and Cu(I) particles was determined and could be used along with the lateral area to calculate the total volume of each of the Cu(0) and Cu(I) species. Section S-9, Figure S-10, shows an example of the calculation of the volume of Cu(0) and Cu(I) at +0.4 V_{RHE} from the full stack results. The calculated volumes at each potential are shown in Table S-2. The volumes of Cu species under various potentials from +0.4 to −0.6 V_{RHE} were calculated by the same method, with results shown in Table S-3. The volume ratios of Cu(0) and Cu(I) at different time periods after specific potentials were applied are displayed in Figure 6a. The Cu(0) particles maintain the same oxidation state at −0.2, −0.4, and −0.6 V_{RHE} (Figure 6, Figure S-9), and the volume ratios were calculated from the full stack (10−40 min) at these three electrode potential values. At +0.4 V_{RHE}, the Cu particles were relatively stable, with a composition of 43(±4)% Cu(0) to 57(±6)% Cu(I) during the first 3−10 min of measurement and 40(±4)% Cu(0) to 60(±6)% Cu(I) during the first 10−40 min of measurement. When the potential was reduced from +0.4 to 0 V_{RHE}, the Cu(I) fraction gradually decreased to <1%. At all potentials more negative than 0 V_{RHE}, the Cu particles consisted of pure Cu(0) within the measurement precision (>99% Cu(0)).

The calculated volumes presented in Figure 6a are consistent with the STXM component thickness maps shown in Figure 5 and Figure S-9. The volumes and volume ratios of Cu(0) and Cu(I) quantitatively show the transition from Cu(I) to Cu(0) during the electrochemical process. Moreover, this can also be straightforwardly confirmed by examining the average spectrum of all the Cu particles at each of the potentials, as shown in Figure 6b. These spectra show that, over the potential sequence, and particularly between +0.2 and 0 V_{RHE}, the particles change from primarily Cu(I) to completely metallic Cu(0).

3. DISCUSSION

Our *in situ* STXM results show that the initially formed, mixed oxidation state Cu particles are converted to exclusively metallic Cu(0) between +0.4 and 0 V_{RHE}—electrode potentials that are several hundred millivolts more positive than where the CO_2R reaction commences. During this reduction process, changes of morphology and oxidation states of the Cu particles were observed during different time periods (0−3, 3−10, 10−40, 40−43 min). Our results show that conversion of some portions of the Cu(I) to Cu(0) is a relatively slow process, continuously occurring over the time period of a few minutes to tens of minutes as the chronoamperometric electrode potential holds are applied. At each potential between +0.4 and 0 V_{RHE}, the Cu(I) particles gradually reduced in size and converted to Cu(0) particles. Moreover, some of the Cu(I) particles completely disappeared during this process rather than converting to metallic Cu, showing there are other reactions in addition to Cu(I)/Cu(0) conversion (see region A1 in Figure 5). Furthermore, some predominantly Cu(I) particles reduced to metallic Cu at different rates at the same electrode potential or did not reduce fully until more negative electrode potentials were applied (Figure 5), suggesting each Cu particle can have significantly different electrochemical responses even under the same applied reaction conditions. These observations show that complicated conditions can be encountered when characterizing Cu-based CO_2R catalysts. Others studies have characterized the Cu materials during the CO_2R process using different *in situ* spectroscopic techniques and found results similar to Figure 6b, whereby Cu(I) decreases and Cu(0) increases as the potential is decreased.[5,45,49] However, the use of spectro-microscopy in this study gave quantitative oxidation state analysis and mapping at a ~40 nm spatial scale, thereby probing the process of Cu(0)/Cu(I) conversion and CO_2R with both morphological and chemical information.

At potentials lower than −0.4 V_{RHE} where CO_2R occurs, only Cu(0) species were observed, which we identify as the active site for CO_2R. The Cu(0) particles were stable during the CO_2R reactions with no detectable changes in oxidation state and morphology of particles within the spectral sensitivity and spatial resolution of STXM (~40 nm). According to the calculated Cu compositions (Figure 6a), the particles are >99% Cu(0) at electrode potentials below 0 V_{RHE}. This strongly

https://doi.org/10.1021/acsnano.3c05964

supports the viewpoint that there are no significant amounts of non-zero-valent Cu species under the electrochemical reducing conditions for the CO_2R reaction.[13−15,49] The results and capabilities of the *in situ* STXM technique brought us to question the assertion across the literature that non-zero-valent Cu species can persist under CO_2R conditions and impact the catalytic processes.[13−15] While every CO_2R catalyst, electrode, and reactor leads to different local chemical reactive environments, we aimed to probe the conditions upon which Cu-oxide species may exist under the CO_2R conditions employed in our *in situ* setup. To accomplish this, in our early *in situ* studies,[34] we prepared a working electrode where we did not limit the amount of Cu that was electrodeposited, leading to the formation of micrometer-scale deposits extending off the surface of the working electrode. This preparation may more closely mimic the thicker catalyst layers used in CO_2R flow cells or membrane electrode assemblies. An STXM image of this electrode is shown in Figure 7a. The chemical mapping of the working electrode after electrodeposition is shown in Figure 7b, while Figure 7c shows Cu oxidation state maps at three different potentials. Upon application of potentials of +1.3 and +0.7 V_{RHE}, the system consisted of a mixture of Cu(0), Cu(I), and Cu(II) species, as expected for Cu-based particles under these electrochemical potentials.[50] Interestingly, after applying a negative electrode potential of −0.5 V_{RHE}, a CO_2R relevant electrode potential, a significant portion of the Cu(I) species remained in the electrode structure. More details of these measurements are provided elsewhere.[30] Under these electrochemically reducing conditions the Cu-oxide species persisted, particularly at locations that extended away from the Au-based working electrode. These regions of the catalyst layer remained unresponsive to changes in electrode potential. In contrast, Cu particles in close proximity to the underlying Au-based working electrode were found to interchange between the metallic Cu(0) and Cu-oxide states as a function of electrode potentials that were more negative and more positive than the reversible potential of the Cu(0)/Cu(I) redox pair, respectively. This persistence of Cu-oxide species at potentials as low as −0.5 V_{RHE} contrasts the results shown in Figure 5, whereby all Cu species were in metallic form at potentials more negative than 0 V_{RHE}. This observation, combined with the lack of electrochemical response observed for the thick catalyst layer regions, led us to conclude that the Cu-oxide species under CO_2R conditions persist because they are electronically isolated from the electrode and therefore have no relevance on electrocatalytic performance. In particular, there is no oxidation state change for the Cu materials located at the top region, while the active Cu materials located at the bottom regions undergo the expected oxidation state changes with varying electrode potentials (Figure 7c). Compared to the relatively thick Cu-based layer, which more closely mimics the practical catalytic electrodes used in CO_2R cells, Cu nanoparticles as the electrocatalysts are favorable due to their superior conductivity and electrochemical activity.

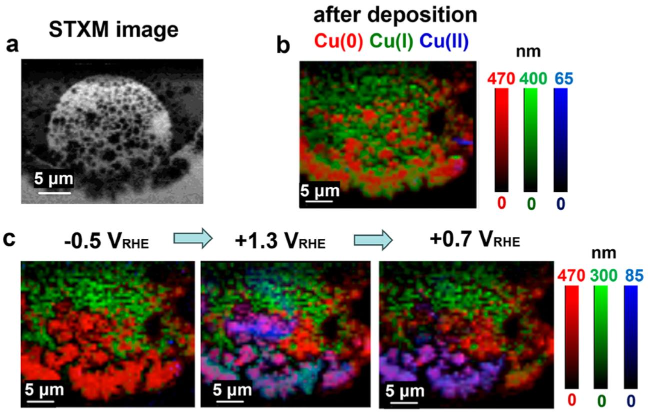

Figure 7. *In situ* STXM to show electronically isolated Cu materials. (a) STXM image (935 eV) for the Cu materials electrodeposited on the whole WE. (b) Cu oxidation state maps of Cu(0) (red), Cu(I) (green), and Cu(II) (blue) of electrodeposited thick Cu materials. (c) Cu oxidation state maps of Cu(0) (red), Cu(I) (green), and Cu(II) (blue) at −0.5, +1.3, and +0.7 V_{RHE} by sequence. More details are presented in ref 34.

The results presented in this work exemplify one of the significant advantages of *in situ* STXM over bulk averaged measurement techniques, such as non spatially resolved X-ray absorption spectroscopy. The latter have shown the presence of oxidized Cu species under CO_2R conditions,[14,15] but cannot provide spatial distinction between regions containing metallic Cu and/or Cu-oxide to validate whether the Cu is electronically active or electronically isolated. The question then arises if small amounts of Cu-oxide can persist under electrochemical CO_2R conditions by being either kinetically or diffusion trapped within the particles. We believe Cu-oxides cannot persist if they are electronically active. Other *in situ* microscopic techniques, including selected area diffraction in a (scanning) transmission electron microscope (TEM or STEM),[16,17,22] have shown that the nanoscale morphology Cu-based particles can rapidly evolve under CO_2R conditions, rendering it very difficult for subsurface Cu-oxide species to remain protected/entrapped at conditions where, thermodynamically, they are unlikely to persist.[51] However, based on the limited spatial resolution (∼40 nm) of the *in situ* STXM used in this work, it is difficult to effectively monitor the nanoscale reconstruction and evolution of Cu particles during CO_2R reactions, a key limitation of current STXM capabilities. This has motivated us to pursue improving the spatial resolution of *in situ* soft X-ray spectro-microscopy by performing *in situ* spectro-ptychography, which provides similar chemical mapping to STXM but at ∼3 times better spatial resolution.[52,53] In our recent *in situ* spectro-ptychography study chemical changes and morphological evolution of a single ∼200 nm sized Cu catalyst particle were tracked from formation to CO_2R conditions, demonstrating the ability to significantly improve upon the spatial resolution limits of STXM and advance *in situ* soft X-ray microscopy beyond the state-of-the-art measurements reported in the present work.[53]

4. CONCLUSIONS

In situ STXM measurements on electrodeposited Cu particles provided detailed, quantitative insight into the morphology and spatially resolved chemical structures present in these catalysts under electrochemical CO_2R conditions. At electrode potentials from +0.4 to 0 V_{RHE}, predominantly Cu(I) particles were converted to metallic Cu. Differences were observed in the electrode potential and/or the rate (time) it took for the particles to become metallic, suggesting that discrete Cu particles have a high degree of heterogeneity in terms of their electrochemical response. However, at CO_2R relevant potentials more negative than 0 V_{RHE}, all of the particles were observed to be completely reduced to metallic Cu within the experimental precision of the measurements (>99%). Very little particle reconstruction was observed, possibly due to the limited spatial resolution capabilities (~40 nm) of the technique. By preparing electrodes with relatively thicker Cu-based electrodeposited catalyst layers, we show that a significant portion of the Cu species can remain in oxidized form at potentials as low as −0.5 V_{RHE}. These Cu-oxide regions in the catalyst layer were found to remain unresponsive to electrode potential, indicating that they were electronically isolated from the underlying working electrode substrate. Thus, we highlight an advantage of *in situ* STXM over bulk-averaged *in situ* measurement techniques in that it can provide spatial and spectroscopic distinction between particles that are electronically connected to the electrode and those that are isolated, rendering them electrocatalytically irrelevant. In this sense, *in situ* STXM, enabled by our custom-designed microfluidic electrochemical device, provides a means for achieving advanced understanding of the morphology and nanometer-scale spatially resolved chemical structures present under CO_2R electrochemical conditions. *In situ* STXM is suitable for electrocatalysis and energy storage (battery) research. The spatial resolution and other capabilities of the technique can be further improved through technological innovations, such as spectro-ptychography and more rapid data acquisition to better follow electrochemically induced changes. For example we recently demonstrated a 3-fold improvement in spatial resolution with similar chemical sensitivity to STXM and improved sensitivity to morphological changes, by performing *in situ* spectro-ptychography on this system using the same *in situ* device.[53]

5. EXPERIMENTAL SECTION

5.1. Catalysis Performance Characterization. The activity and selectivity of the Cu particles used in this work toward electrochemical CO_2R was tested. Cu particle coated working electrodes were prepared by electrodepositing a solution of 5 mM $CuSO_4$ and 5 mM KCl on an Au-coated graphite foil by running three cycles of CV from 0 to +0.4 V versus the reversible hydrogen electrode (V_{RHE}) with a scan rate of 20 mV/s. This is identical to the process used to prepare Cu catalysts in the *in situ* STXM cell. The electrodeposited Cu electrode was used as the working electrode for electrochemical CO_2 reduction and tested in a custom-built two-compartment electrolyte membrane separated cell that has been reported previously[40,41] (Figure S-1a). The geometric area of the working electrode was 5.7 cm^2. The electrolyte compartments of the working and counter electrode were filled with CO_2-saturated 0.1 M $KHCO_3$ (5 mL). CO_2 was flowed continuously through the catholyte and anolyte chambers at 20 sccm throughout the course of the experiment. A Pt foil was used as the counter electrode, and a Ag/AgCl electrode was used as the reference electrode. The Ag/AgCl reference electrode was calibrated versus a homemade reversible hydrogen electrode (RHE), and the reported potentials are versus RHE. The catholyte and anolyte chambers were separated by an ion exchange membrane (Selemion AMV, AGC Inc.). Catalysts were tested by chronoamperometric measurements at various electrochemical potentials, −0.2, −0.4, and −0.6 to −0.8 V_{RHE}. The effluent gas from the catholyte compartment was fed to a gas chromatograph (GC), and the collected electrolyte was tested using nuclear magnetic resonance (NMR) for liquid product identification and quantitation to determine Faradaic efficiencies. CV was conducted to check the potentials of Cu oxidation and reduction peaks in CO_2-saturated 0.1 M $KHCO_3$ in the two-compartment membrane cell (Figure S-1a).

5.2. *In Situ* Microfluidic-Based Electrochemical Device. Figure 2 presents the microfluidic-based flow electrochemical device used for *in situ* flow electrochemical STXM experiments. The *in situ* device consists of a machined printed circuit board (PCB), a polydimethylsiloxane (PDMS)/glass cell equipped with the electrochemical *in situ* chips (PDMS cell), and a poly(methyl methacrylate) (PMMA) backplate (PMMA plate) (Figure 2a).[34,35] The microfluidic PDMS cell contains four flow tubes and microfluidic channels, shown as dotted lines on the PDMS cell, which serve as two inlets and two outlets to connect to the assembled *in situ* microchip reactor (Figure 2b, Norcada Inc., Edmonton, Canada, https://www.norcada.com). The flow tubes can be connected to one or more fluid circulation devices (we use syringe pumps, but pressure pumps could also be used) to establish a stable flow of one or more electrolytic fluids to the *in situ* chips. Electrochemical reactions can then be performed by applying suitable potentials to the three electrodes on base chip E (Figure 2c), which are connected to a potentiostat through the PCB traces and a four-pin connector on the PC board. Spacer chip F (Figure 2b) has a predeposited 1 μm spacer defining the height of the electrolyte flow channel within the microchip setup (chip F with a 0.5 mm spacer is also available, resulting in a thinner electrolyte layer). The working electrode, counter electrode, and reference electrodes on base chip E are all Au (Figure 2c). The darker circles on the working electrode and counter electrode are thinner regions which reduce X-ray absorption arising from the electrode thickness. The Au reference electrode acts as a pseudo-reference electrode, such that all potentials measured are voltage versus the Au pseudo-reference (denoted V_{Au}). The open-circuit potential (OCP) was stable (~−0.048 ± 0.004 V_{Au}) in CO_2-saturated 0.1 M $KHCO_3$ with electrodeposited Cu on the Au working electrode (Figure S-2d). External CV measurements conducted in a two-compartment cell using a calibrated Ag/AgCl electrode (Figure S-1e) enabled us to convert from potentials measured relative to the Au pseudo-reference electrode to V_{RHE} using the well-defined Cu redox peaks. The calibration yielded a value of $V_{RHE} = V_{Au} + 0.40$. All potentials reported in this work are relative to RHE, unless stated otherwise.

When the *in situ* device is assembled, the PDMS/glass cell is kept in place in the machined PCB frame by a PMMA back-plate. Electrical connections between the on-chip electrodes and Cu traces on the PC board are made using Cu clips soldered to the PCB traces. For the experiments, the *in situ* microfluidic-based flow electrochemical device is connected to a potentiostat (Emstat4 (PalmSens) or Ivium PocketStat, https://www.ivium.com/instruments/) to control potential and monitor current while one or more of the fluid lines is connected to a syringe pump (New Era, https://www.syringepump.com/) to establish a stable electrolyte flow rate, typically 10−50 μL/h.

5.3. *In Situ* Device Setup and Mounting in STXM. First, the electrolytes used in *in situ* experiments are prepared and loaded into 1 mL syringes. Bubbles are removed by pushing/withdrawing the syringe. The syringe with the electrolyte is connected to the *in situ* device using Tefzel tubes (Idex, www.idex-hs.com) with an inner diameter (i.d.) of 0.040 in. and outer diameter of 0.0625 in.) [NB: improved performance was found after these experiments by using a narrower 0.010 in. i.d. tubing]. The syringe plunger is pushed manually to fill the tubes with electrolyte. Then the filled tubing is connected to the assembled *in situ* device and the syringe plunger is placed into the syringe pump. A flow rate of 25 μL/h for 10 min is used to slowly fill the *in situ* device with electrolyte. The filling process is always conducted under an optical microscope, in order to confirm that the electrolyte completely fills the window region (Figure S-2). Once the three-electrode region (Figure 2c) is filled with the electrolyte, the *in situ* device is connected to the potentiostat. The open-circuit potential should be close to ~+0.35 V_{RHE} and stable within ±0.004 V, confirming proper connections and electrochemical activity. These procedures verify good electrical connections and steady electrolyte flow with no problems such as liquid leaking, channel blocking due to bubbles, or cable disconnection.

Then the *in situ* device is loaded into the STXM. First, the connections to the potentiostat and syringe pump are disconnected to simplify device insertion into the STXM. The *in situ* device, connected only to the electrolyte tubing, is moved with caution from the optical microscope to the STXM chamber and inserted through a 4.5 in. flange. Note, since these measurements were first made, the fluid line and electrical connections have been modified to be implemented on a 2.75 in. Conflat flange, which enables compatibility with most modern STXMs. In the chamber, the *in situ* device is mounted in the three-pin sample kinematic holder, and then the potentiostat and syringe pump are reconnected. The syringe pump is turned on with a flow rate of 25 μL/h to keep a stable electrolyte flow through the *in situ* device. The electrolyte tubes and potentiostat cables are organized in the STXM chamber and stabilized using Kapton tape to attach them to a suitable position in the chamber to avoid interfering with STXM operations such as sample scanning.

After the *in situ* device is loaded in the STXM, the air in the tank is replaced with He gas by displacing the air at a slow rate (~10 min). After achieving a plateau in X-ray transmission, the He gas flow is stopped and the STXM chamber is closed. Note that this procedure is routine at the CLS ambient STXM, but not possible at some other facilities, due to a minimum vacuum requirement. STXM imaging was used to locate the SiN_x window (240 μm × 120 μm) and to make sure there are no bubbles in the three-electrode area that occasionally occur in the process of moving and loading the *in situ* device into the STXM. The signal from X-rays transmitted through the SiN_x windows and electrolyte is measured and compared with the incident X-ray intensity measured in one of the holes in the *in situ* device (Figure 2d) in order to evaluate the absorption (optical density, OD), which in most spectral regimes is dominated by absorption by the water. Comparison to the known X-ray transmission properties of the SiN_x windows and water allows determination of the thickness of the electrolyte, which was between 2 and 5 μm, depending on the spacer used (0.5, 1, 1.5 μm), syringe pump flow rate, and i.d. of the electrolyte tubing. An electrolyte layer as thin as ~1.6 μm can be achieved. In this work a 1 μm spacer was used. If the electrolyte layer is thick (>4 μm), X-rays at the Cu 2p edge (~930 eV) cannot transmit through the electrolyte and STXM measurements cannot be performed. After the liquid thickness is measured, electrochemical experiments are performed on the three-electrode area by applying potentials and measuring currents using a potentiostat.

5.4. Electrodeposition of Cu Catalyst Particles. Copper nanoparticles were electrodeposited from a solution of 5 mM $CuSO_4$ and 5 mM KCl onto the Au working electrode of the *in situ* microchip cell. The electrodeposition solution concentrations and conditions were chosen based on previous reports[16,17] to target particles in the range of 300−500 nm diameter that are relevant for CO_2R and STXM measurements. After setting up the *in situ* device as described in Section 5.3, the electrodeposition was carried out by performing three cyclic voltammetry cycles between 0 and +0.4 V_{RHE} with a scan rate of 20 mV/s. This is the same protocol as used to prepare the electrode for the catalyst performance measurements described in Section 5.1. The as-deposited Cu particles are then characterized using STXM to gain insight into the morphology and chemical structure (i.e., oxidation state) distributions (see Section S-3, Figure S-3). STXM measurements at this step should be as fast as possible because some Cu particles will slowly disappear by dissolution into the 5 mM $CuSO_4$/KCl electrolyte, which has a measured pH of 6.1. This could be caused by slow conversion of Cu(I) to Cu(II) in the mildly acidic environment under open-circuit potential conditions (ca. +0.35 ± 0.004 V_{RHE} under *in situ* conditions), as Cu(I) is not stable at lower pH values,[54] followed by Cu(II) dissolution into the electrolyte. This phenomenon has been observed several times in our *in situ* experiments.

Once a region with particles of suitable thickness (50−200 nm) and size (50−600 nm) is identified and oxidation states are determined, the $CuSO_4$/KCl electrolyte is displaced by CO_2-saturated 0.1 M $KHCO_3$ for subsequent *in situ* STXM experiments under CO_2R conditions. In the CO_2-saturated 0.1 M $KHCO_3$ electrolyte, the Cu particles are more stable, as the pH is closer to neutral (pH 6.8). Therefore, changing the electrolyte from $CuSO_4$/KCl to CO_2-saturated 0.1 M $KHCO_3$ is done as fast as possible to avoid loss of the deposited Cu particles.

5.5. *In Situ* STXM under CO_2R Conditions. The CO_2-saturated 0.1 M $KHCO_3$ is prepared just before the *in situ* STXM experiments by bubbling CO_2 gas into a 0.1 M $KHCO_3$ solution for 20 min in a septum-sealed vial. After Cu *in situ* electrodeposition (Section 5.4) the electrolyte is changed to CO_2-saturated 0.1 M $KHCO_3$. Deionized water is first used to flush the $CuSO_4$/KCl out of the *in situ* microchip device. Then the CO_2-saturated 0.1 M $KHCO_3$ electrolyte is continuously filled using a 25 μL/h flow rate. Changing the electrolyte takes around 20 min. After electrolyte changes, there is no STXM-detectible Cu^{2+} signal in the electrolyte. *In situ* STXM measurements were conducted using a series of chronoamperometry (CA) potential sequences. Before all measurements, CA at +0.4 V_{RHE} was applied for 30 s (to ensure the catalyst was always in the same starting state) followed by a cathodic step to the electrode potential at which STXM was conducted. STXM measurements were conducted sequentially (with +0.4 V_{RHE} for 30 s in between each) at +0.4, +0.3, +0.2, +0.1, 0, −0.2, −0.4, and −0.6 V_{RHE}. The CA current−time plots are presented in Figure S-4. During CA at each potential, the current was continuously recorded and several STXM measurements were made in sequence. The sequence consisted of (1) STXM image at 933.5 eV; (2) four-energy stack measurement that enabled differentiation between the different oxidation states of Cu present in the materials; (3) 53-energy Cu 2p stack; and (4) STXM image at 933.5 eV for comparison with the first STXM image measured. In all this took ~43 m at each potential which enabled time-dependent monitoring of morphology and chemical structure changes to the Cu particles under controlled electrode potentials. Potentials more negative than −0.6 V_{RHE} were not applied, as bubble formation would render the STXM measurements unstable. Gas generation by CO_2R to gas phase products or water reduction to H_2 occasionally created large bubbles which occupied the three-electrode region, leading to a disconnection of the working electrode that stopped the electrochemical reactions. Generally, electrode potentials less negative than −0.6 V_{RHE} did not generate gas bubbles in the *in situ* setup. Following CA potentials and STXM measurement, cyclic voltammograms were collected (Figure S-1c).

5.6. STXM Measurements and Analysis. STXM imaging and spectromicroscopy were performed using the spectromicroscopy beamline (SM) 10ID-1 at the Canadian Light Source (CLS, Saskatoon, Canada). Details of the ambient STXM,[55] beamline,[56] and operating procedures[36] have been presented elsewhere. Briefly, the monochromatic X-ray beam was focused to a ~40 nm spot by a Fresnel zone plate (ZP). The sample was positioned at the focal point of the X-ray beam. Images were measured by (*x*,*y*) raster scanning the sample while recording the transmitted X-ray intensity pixel by pixel in a single-photon counting mode using a phosphor/photomultiplier single X-ray counting detector. The energy scale was calibrated by recording the Ne 1s spectrum of the Ne gas.[57]

Four types of STXM measurements were used in this work: STXM point scan, STXM image, STXM full stack, and STXM four-energy stack. The STXM point scan measures the transmission spectrum at one or more points on a sample over a user-specified photon energy range. In this work, point scans at the Cu 2p edge from 920 to 965 eV were measured at the position of one of the holes drilled through the *in situ* device to obtain the incident X-ray (I_o) signal (Figure S-5a,b). The difference in the X-ray intensity between the I_o spectrum and that measured through the electrolyte in the cell corresponds to the X-ray absorption by the SiN_x windows and the electrolyte (Figure S-5c). If the material composition and density are known, the net X-ray absorption, given by OD = $-\ln(I/I_o)$, is directly related to the thickness. After subtracting the OD of 150 nm SiNx, the remaining OD represents the X-ray absorption of the electrolyte. The electrolyte is mostly water, so the X-ray absorption properties of H_2O in the 900−1000 eV range were used to calculate the thickness of electrolyte in the window region, which was ~1.6 μm (Section S-5, Figure S-5d). STXM images at a single photon energy were measured by scanning the sample while recording the transmitted X-ray intensity pixel by pixel. An STXM full stack involved a sequence of STXM images collected at various photon energies (also known as stacks[36]) to provide spatially resolved spectroscopic information about the sample. In this work, a 53-energy Cu 2p stack spanning 920 to 965 eV (taking a total of ~30 min) was used. An STXM 4-E stack (~7 min) was also used to conduct chemical speciation of the sample in an accelerated fashion. It measured images at 920 (pre-edge), 933.5 (Cu(I) and Cu(0)), 937 (Cu(I)), and 960 eV (post-edge) and provides the same spectroscopic information as the STXM full stack (Figure S-6). Further details of the STXM measurements are presented in Table S-1.

STXM is typically regarded as a technique that causes limited radiation damage,[58−60] especially relative to analytical electron microscopies.[58−62] Experimental evidence, demonstrating that the results from this *in situ* STXM study of Cu electrocatalysts are not significantly affected by radiation damage, is presented in Supporting Information Section S-11.

All STXM data were analyzed using aXis2000 software.[63] The images in a stack typically drift by a few hundred nanometers over a 40−80 eV scan range. Therefore, the stacks were aligned to ∼2 nm registry using a Fourier cross-correlation method. The transmission signal (I) of the aligned stack was converted to optical density (OD) using the Beer−Lambert law: $OD_{(x,y)} = -\ln(I_{(x,y)}/I_o)$, where $I_{(x,y)}$ is the X-ray intensity transmitted though the (x,y) point on the sample and I_o is the incident X-ray intensity measured off the sample but where the X-rays transmit through all other parts of the X-ray path (optics, windows, zone plate, detector) and the sample support (the electrolyte and a 150 nm SiN_x window). After OD conversion, the Cu 2p X-ray absorption spectra (XAS) of selected areas (many pixels, which are not necessarily contiguous, but with similar Cu L_3 spectra) were extracted from the STXM stacks using methods described in greater detail below.

A fitting procedure, based on the singular value decomposition (SVD) matrix method,[64] was used to analyze the stacks. The SVD routine fits the NEXAFS spectrum at each pixel to a user-identified set of reference spectra, which can be derived from the spectroscopy of pure reference compounds (external) or to spectra extracted from the measured stack (internal). The result of an SVD fitting is a set of component maps (spatial distributions), one for each component, along with the residual of the fit.[64] For quantitative analysis, the external reference spectra are converted to an absolute intensity scale, optical density per nm (OD1),[36,63,64] by scaling the spectrum such that the intensity in the pre-edge and far-continuum (>30 eV above the edge) match the elemental response for 1 nm thickness of the known composition and density of the reference material. The latter are calculated using parameters from the Centre for X-ray Optics database [https://henke.lbl.gov/optical_constants/]. The gray scale of the component maps derived using OD1 reference spectra is an estimate of the thickness of that component at each pixel in the region analyzed. To confirm the validity of the spectro-microscopy fitting procedure, spectra are extracted from specific areas of a stack, identified based on morphology and/or spectral similarity, and then subjected to a spectral curve-fitting procedure using SVD. When reference spectra on OD1 intensity scales are used in an SVD curve fit, the gray scale of the component maps of each spectral component is an estimate of the average thickness in nanometers of that component in the area from which the spectra were extracted.

ASSOCIATED CONTENT

Data Availability Statement

The data sets generated during and/or analyzed during the current study are available from the corresponding author on reasonable request.

Supporting Information

The Supporting Information is available free of charge at https://pubs.acs.org/doi/10.1021/acsnano.3c05964.

> Additional experimental details (potential calibration, electrolyte filling process, details of *in situ* electrodeposition, summary of *in situ* measurements), details of the STXM measurements and data analysis, further supporting results (quantitative analysis details, quantitative calculation details, evidence of no obvious radiation damage) (PDF)

AUTHOR INFORMATION

Corresponding Author

Drew Higgins − *Chemical Engineering, McMaster University, Hamilton, Ontario, Canada L8S 4M1;* orcid.org/0000-0002-0585-2670; Email: higgid2@mcmaster.ca

Authors

Chunyang Zhang − *Chemical Engineering and Chemistry & Chemical Biology, McMaster University, Hamilton, Ontario, Canada L8S 4M1*

Haytham Eraky − *Chemistry & Chemical Biology, McMaster University, Hamilton, Ontario, Canada L8S 4M1*

Shunquan Tan − *Chemical Engineering, McMaster University, Hamilton, Ontario, Canada L8S 4M1*

Adam Hitchcock − *Chemistry & Chemical Biology, McMaster University, Hamilton, Ontario, Canada L8S 4M1;* orcid.org/0000-0002-1598-7886

Complete contact information is available at: https://pubs.acs.org/10.1021/acsnano.3c05964

Notes

The authors declare no competing financial interest.

This work was submitted as a preprint version to ChemRxiv to solicit feedback from the scientific community and establish priority for publication as this is a rapidly evolving field of research.[65]

ACKNOWLEDGMENTS

Measurements were made at the ambient STXM on beamline 10ID1 at the CLS. The CLS is funded by CFI, NSERC, NRC, CIHR, the Government of Saskatchewan, and the University of Saskatchewan. We thank the beamline staff at CLS-SM (Jian Wang). We especially thank Martin Obst and Pablo Ingino (University Bayreuth) for sharing design details; Paul Gatt and Michael Clarke (Chemical Engineering, McMaster); and Prof. Jose Moran-Mirabal and their students (Chemistry & Chemical Biology, McMaster) for assistance with device development and fabrication. This research was supported by the Natural Sciences and Engineering Research Council (NSERC) Discovery Grant program, the National Research Council of Canada (NRC) Materials for Clean Fuels Challenge program, and TotalEnergies.

REFERENCES

(1) Wang, P.; Yang, H.; Tang, C.; Wu, Y.; Zheng, Y.; Cheng, T.; Davey, K.; Huang, X.; Qiao, S. Z. Boosting electrocatalytic CO_2−to−ethanol production via asymmetric C−C coupling. *Nat. Commun.* **2022**, *13*, 1−11.

(2) Zhang, C.; Shahcheraghi, L.; Ismail, F.; Eraky, H.; Yuan, H.; Hitchcock, A. P.; Higgins, D. Chemical Structure and Distribution in Nickel−Nitrogen−Carbon Catalysts for CO_2 Electroreduction Identified by Scanning Transmission X-ray Microscopy. *ACS catalysis* **2022**, *12*, 8746−8760.

(3) Chou, T. C.; Chang, C. C.; Yu, H. L.; Yu, W. Y.; Dong, C. L.; Velasco-Vélez, J. J.; Chuang, C. H.; Chen, L. C.; Lee, J. F.; Chen, J. M.; Wu, H. L. Controlling the oxidation state of the Cu electrode and reaction intermediates for electrochemical CO_2 reduction to ethylene. *J. Am. Chem. Soc.* **2020**, *142*, 2857−2867.

(4) Wei, P.; Gao, D.; Liu, T.; Li, H.; Sang, J.; Wang, C.; Cai, R.; Wang, G.; Bao, X. Coverage-driven selectivity switch from ethylene to

acetate in high-rate CO2/CO electrolysis. *Nat. Nanotechnol.* **2023**, *18*, 299−306.

(5) Yang, Y.; Roh, I.; Louisia, S.; Chen, C.; Jin, J.; Yu, S.; Salmeron, M. B.; Wang, C.; Yang, P. Operando Resonant Soft X-ray Scattering Studies of Chemical Environment and Interparticle Dynamics of Cu Nanocatalysts for CO_2 Electroreduction. *J. Am. Chem. Soc.* **2022**, *144*, 8927−8931.

(6) Lu, C.; Li, X.; Wu, Q.; Li, J.; Wen, L.; Dai, Y.; Huang, B.; Li, B.; Lou, Z. Constructing surface plasmon resonance on Bi2WO6 to boost high-selective CO2 reduction for methane. *ACS Nano* **2021**, *15*, 3529−3539.

(7) Wu, Q.; Liu, C.; Su, X.; Yang, Q.; Wu, X.; Zou, H.; Long, B.; Fan, X.; Liao, Y.; Duan, L.; Quan, Z. Defect-Engineered Cu-Based Nanomaterials for Efficient CO2 Reduction over Ultrawide Potential Window. *ACS Nano* **2023**, *17*, 402−410.

(8) Watkins, N. B.; Wu, Y.; Nie, W.; Peters, J. C.; Agapie, T. In Situ Deposited Polyaromatic Layer Generates Robust Copper Catalyst for Selective Electrochemical CO_2 Reduction at Variable pH. *ACS Energy Letters* **2023**, *8*, 189−195.

(9) Zhu, C.; Zhao, S.; Shi, G.; Zhang, L. Structure-Function Correlation and Dynamic Restructuring of Cu for Highly Efficient Electrochemical CO2 Conversion. *ChemSusChem* **2022**, *15*, e202200068.

(10) Eilert, A.; Cavalca, F.; Roberts, F. S.; Osterwalder, J.; Liu, C.; Favaro, M.; Crumlin, E. J.; Ogasawara, H.; Friebel, D.; Pettersson, L. G.; Nilsson, A. Subsurface oxygen in oxide-derived copper electrocatalysts for carbon dioxide reduction. *journal of physical chemistry letters* **2017**, *8*, 285−290.

(11) Wang, H. Y.; Soldemo, M.; Degerman, D.; Lömker, P.; Schlueter, C.; Nilsson, A.; Amann, P. Direct Evidence of Subsurface Oxygen Formation in Oxide-Derived Cu by X-ray Photoelectron Spectroscopy. *Angew. Chem.* **2022**, *61*, e202111021.

(12) Fields, M.; Hong, X.; Nørskov, J. K.; Chan, K. Role of subsurface oxygen on Cu surfaces for CO_2 electrochemical reduction. *J. Phys. Chem. C* **2018**, *122*, 16209−16215.

(13) Scott, S. B.; Hogg, T. V.; Landers, A. T.; Maagaard, T.; Bertheussen, E.; Lin, J. C.; Davis, R. C.; Beeman, J. W.; Higgins, D.; Drisdell, W. S.; Hahn, C.; et al. Absence of oxidized phases in Cu under CO reduction conditions. *ACS Energy Letters* **2019**, *4*, 803−804.

(14) Lum, Y.; Ager, J. W. Stability of residual oxides in oxide-derived copper catalysts for electrochemical CO_2 reduction investigated with ^{18}O labeling. *Angew. Chem.* **2018**, *57*, 551−554.

(15) Jiang, P.; Prendergast, D.; Borondics, F.; Porsgaard, S.; Giovanetti, L.; Pach, E.; Newberg, J.; Bluhm, H.; Besenbacher, F.; Salmeron, M. Experimental and theoretical investigation of the electronic structure of Cu_2O and CuO thin films on Cu (110) using x-ray photoelectron and absorption spectroscopy. *J. Chem. Phys.* **2013**, *138*, No. 024704.

(16) Grosse, P.; Yoon, A.; Rettenmaier, C.; Herzog, A.; Chee, S. W.; Roldan Cuenya, B. Dynamic transformation of cubic copper catalysts during CO_2 electroreduction and its impact on catalytic selectivity. *Nat. Commun.* **2021**, *12*, 6736.

(17) Arán-Ais, R. M.; Rizo, R.; Grosse, P.; Algara-Siller, G.; Dembélé, K.; Plodinec, M.; Lunkenbein, T.; Chee, S. W.; Cuenya, B. R. Imaging electrochemically synthesized Cu_2O cubes and their morphological evolution under conditions relevant to CO_2 electroreduction. *Nat. Commun.* **2020**, *11*, 1−8.

(18) Handoko, A. D.; Wei, F.; Jenndy; Seh, Z. W.; Yeo, B. S. Understanding heterogeneous electrocatalytic carbon dioxide reduction through operando techniques. *Nature Catalysis* **2018**, *1*, 922−934.

(19) Hasa, B.; Zhao, Y.; Jiao, F. In Situ/Operando Characterization Techniques of Electrochemical CO_2 Reduction. *Annu. Rev. Chem. Biomol. Eng.* **2023**, *14*, 1.

(20) Zheng, T.; Liu, C.; Guo, C.; Zhang, M.; Li, X.; Jiang, Q.; Xue, W.; Li, H.; Li, A.; Pao, C. W.; Xiao, J. Copper-catalysed exclusive CO2 to pure formic acid conversion via single-atom alloying. *Nat. Nanotechnol.* **2021**, *16*, 1386−1393.

(21) Li, X.; Yang, X.; Zhang, J.; Huang, Y.; Liu, B. In situ/operando techniques for characterization of single-atom catalysts. *ACS Catal.* **2019**, *9*, 2521−2531.

(22) Yang, Y.; Louisia, S.; Yu, S.; Jin, J.; Roh, I.; Chen, C.; Fonseca Guzman, M. V.; Feijóo, J.; Chen, P. C.; Wang, H.; Pollock, C. J.; et al. Operando studies reveal active Cu nanograins for CO_2 electroreduction. *Nature* **2023**, *614*, 262−269.

(23) Abdellah, A.; Ismail, F.; Siig, O.; Yang, J.; Andrei, C.; DiCecco, L.; Rakhsha, A.; Salem, K.; Grandfield, K.; Bassim, N.; Black, R.; Kastlunger, G.; Soleymani, L.; Higgins, D. In-Situ Liquid Phase Transmission Electron Microscopy and Electron Diffraction Provides Mechanistic Insight into Electrochemical CO2 Reduction on Palladium/Palladium Hydride Catalysts. 2023, 10.26434/chemrxiv-2023-t0b00. *ChemRxiv*. (https://chemrxiv.org/engage/chemrxiv/article-details/63ced2cb246f166af7ca1b5e) (accessed Jan 24, 2023).

(24) Chee, S. W.; Lunkenbein, T.; Schlögl, R.; Cuenya, B. R. In situ and operando electron microscopy in heterogeneous catalysis—insights into multi-scale chemical dynamics. *J. Phys.: Condens. Matter* **2021**, *33*, 153001.

(25) Hwang, S.; Chen, X.; Zhou, G.; Su, D. In situ transmission electron microscopy on energy-related catalysis. *Adv. Energy Mater.* **2020**, *10*, 1902105.

(26) Guay, D.; Stewart-Ornstein, J.; Zhang, X.; Hitchcock, A. P. In situ spatial and time-resolved studies of electrochemical reactions by scanning transmission X-ray microscopy. *Analytical chemistry* **2005**, *77*, 3479−3487.

(27) Bozzini, B.; D'Urzo, L.; Gianoncelli, A.; Kaulich, B.; Kiskinova, M.; Prasciolu, M.; Tadjeddine, A. In situ soft X-ray dynamic microscopy of electrochemical processes. *Electrochem. Commun.* **2008**, *10*, 1680−1683.

(28) de Groot, F. M.; de Smit, E.; van Schooneveld, M. M.; Aramburo, L. R.; Weckhuysen, B. M. In-situ scanning transmission X-ray microscopy of catalytic solids and related nanomaterials. *ChemPhysChem* **2010**, *11*, 951−962.

(29) Gianoncelli, A.; Kaulich, B.; Kiskinova, M.; Mele, C.; Prasciolu, M.; Sgura, I.; Bozzini, B. Fabrication and testing of an electrochemical microcell for in situ soft X-ray microspectroscopy measurements. *Journal of Physics: Conference Series.* **2013**, *425*, 182010.

(30) Prabu, V.; Obst, M.; Hosseinkhannazer, H.; Reynolds, M.; Rosendahl, S.; Wang, J.; Hitchcock, A. P. Instrumentation for in situ flow electrochemical scanning transmission X-ray microscopy (STXM). *Rev. Sci. Instrum.* **2018**, *89*, No. 063702.

(31) Obst, M.; Ingino, P.; Hitchcock, A.; Prabu, V.; Picard, A. Redox-chemistry of environmental biofilms probed on the submicron scale by *in-situ* electrochemical scanning transmission (soft) X-ray microscopy. *Microscopy and Microanalysis* **2018**, *24*, 502−505.

(32) Beheshti Askari, A.; Al Samarai, M.; Morana, B.; Tillmann, L.; Pfänder, N.; Wandzilak, A.; Watts, B.; Belkhou, R.; Muhler, M.; DeBeer, S. *In situ* X-ray microscopy reveals particle dynamics in a NiCo dry methane reforming catalyst under operating conditions. *ACS Catal.* **2020**, *10*, 6223−6230.

(33) Arul, K. T.; Chang, H. W.; Shiu, H. W.; Dong, C. L.; Pong, W. F. A review of energy materials studied by in situ/operando synchrotron x-ray spectro-microscopy. *J. Phys. D: Appl. Phys.* **2021**, *54*, 343001.

(34) Hitchcock, A. P.; Zhang, C.; Eraky, H.; Shahcheraghi, L.; Ismail, F.; Higgins, D. *In-situ* and Operando Studies with Soft X-Ray Transmission Spectromicroscopy. *Microscopy and Microanalysis* **2021**, *27*, 59−60.

(35) Zhang, C.; Eraky, H.; Ingino, P.; Obst, W.; Jian; Higgins, D.; Hitchcock, A. P. *In-situ* STXM Characterization of Cu/Cu_2O Electrocatalysts for CO_2 Reduction. *AIP Conf. Proc.* **2023**, *2990*, No. 020011.

(36) Hitchcock, A. P. Soft X-Ray Imaging and Spectro-microscopy. In *Handbook of Nanoscopy*; Wiley: Weinheim, Germany, 2012; pp 745−791.

(37) Ade, H.; Hitchcock, A. P. NEXAFS microscopy and resonant scattering: Composition and orientation probed in real and reciprocal space. *Polymer* **2008**, *49*, 643−675.

(38) Lee, S. H.; Lin, J. C.; Farmand, M.; Landers, A. T.; Feaster, J. T.; Avilés Acosta, J. E.; Beeman, J. W.; Ye, Y.; Yano, J.; Mehta, A.; Davis, R. C.; et al. Oxidation state and surface reconstruction of Cu under CO_2 reduction conditions from in situ X-ray characterization. *J. Am. Chem. Soc.* **2021**, *143*, 588−592.

(39) Chourasia, A. K.; Pathak, A. D.; Bongu, C.; Manikandan, K.; Praneeth, S.; Naik, K. M.; Sharma, C. S. In Situ/Operando Characterization Techniques: The Guiding Tool for the Development of Li−CO_2 Battery. *Small Methods* **2022**, *6*, 2200930.

(40) Fang, L.; Seifert, S.; Winans, R. E.; Li, T. Understanding synthesis and structural variation of nanomaterials through in situ/operando XAS and SAXS. *Small* **2022**, *18*, 2106017.

(41) Celorrio, V.; Leach, A. S.; Huang, H.; Hayama, S.; Freeman, A.; Inwood, D. W.; Fermin, D. J.; Russell, A. E. 2021. Relationship between Mn oxidation state changes and oxygen reduction activity in (La, Ca) MnO_3 as probed by in situ XAS and XES. *ACS Catal.* **2021**, *11*, 6431−6439.

(42) Fan, Z.; Zhang, L.; Baumann, D.; Mei, L.; Yao, Y.; Duan, X.; Shi, Y.; Huang, J.; Huang, Y.; Duan, X. In situ transmission electron microscopy for energy materials and devices. *Adv. Mater.* **2019**, *31*, 1900608.

(43) Huang, H.; Wang, J.; Yang, X.; Hu, R.; Liu, J.; Zhang, L.; Zhu, M. Unveiling the advances of nanostructure design for alloy-type potassium-ion battery anodes via in situ TEM. *Angew. Chem.* **2020**, *132*, 14612−14618.

(44) Kuhl, K. P.; Cave, E. R.; Abram, D. N.; Jaramillo, T. F. New Insights into the Electrochemical Reduction of Carbon Dioxide on Metallic Copper Surfaces. *Energy Environ. Sci.* **2012**, *5*, 7050−7059.

(45) Higgins, D.; Landers, A. T.; Ji, Y.; Nitopi, S.; Morales-Guio, C. G.; Wang, L.; Chan, K.; Hahn, C.; Jaramillo, T. F. Electrochemical Carbon Dioxide Reduction toward Carbonyls Using Copper Silver Thin Films with Interphase Miscibility. *ACS Energy Lett.* **2018**, *3*, 2947−2955.

(46) Wang, L.; Nitopi, S. A.; Bertheussen, E.; Orazov, M.; Morales-Guio, C. G.; Liu, X.; Higgins, D. C.; Chan, K.; Nørskov, J. K.; Hahn, C.; Jaramillo, T. F. Electrochemical carbon monoxide reduction on polycrystalline copper: Effects of potential, pressure, and pH on selectivity toward multicarbon and oxygenated products. *ACS Catal.* **2018**, *8*, 7445−7454.

(47) Morales-Guio, C. G.; Cave, E. R.; Nitopi, S. A.; Feaster, J. T.; Wang, L.; Kuhl, K. P.; Jackson, A.; Johnson, N. C.; Abram, D. N.; Hatsukade, T.; Hahn, C. Improved CO_2 reduction activity towards C2+ alcohols on a tandem gold on copper electrocatalyst. *Nature Catalysis* **2018**, *1*, 764−771.

(48) Zheng, Y.; Zhang, J.; Ma, Z.; Zhang, G.; Zhang, H.; Fu, X.; Ma, Y.; Liu, F.; Liu, M.; Huang, H. Seeded growth of gold−copper janus nanostructures as a tandem catalyst for efficient electroreduction of CO_2 to C2+ products. *Small* **2022**, *18*, 2201695.

(49) Velasco-Velez, J. J.; Mom, R. V.; Sandoval-Diaz, L. E.; Falling, L. J.; Chuang, C. H.; Gao, D.; Jones, T. E.; Zhu, Q.; Arrigo, R.; Roldan Cuenya, B.; Knop-Gericke, A. Revealing the active phase of copper during the electroreduction of CO_2 in aqueous electrolyte by correlating in situ X-ray spectroscopy and in situ electron microscopy. *ACS Energy Letters* **2020**, *5*, 2106−2111.

(50) Reyter, D.; Odziemkowski, M.; Bélanger, D.; Roué, L. Electrochemically activated copper electrodes: surface characterization, electrochemical behavior, and properties for the electroreduction of nitrate. *J. Electrochem. Soc.* **2007**, *154*, K36.

(51) Fields, M.; Hong, X.; Nørskov, J. K.; Chan, K. Role of subsurface oxygen on Cu surfaces for CO2 electrochemical reduction. *J. Phys. Chem. C* **2018**, *122*, 16209−16215.

(52) Shapiro, D. A.; Yu, Y. S.; Tyliszczak, T.; Cabana, J.; Celestre, R.; Chao, W.; Kaznatcheev, K.; Kilcoyne, A. D.; Maia, F.; Marchesini, S.; Meng, Y. S.; et al. Chemical composition mapping with nanometre resolution by soft X-ray microscopy. *Nat. Photonics* **2014**, *8*, 765−769.

(53) Zhang, C.; Mille, N.; Eraky, H.; Stanescu, S.; Swaraj, S.; Belkhou, R.; Higgins, D.; Hitchcock, A. Copper CO_2 Reduction Electrocatalysts Studied by *In-situ* Soft X-ray Spectro-Ptychography. *Cell Reports Physical Sciences* **2023** (in press). DOI: 10.1016/j.xcrp.2023.101665

(54) Beverskog, B.; Puigdomenech, I. Revised Pourbaix Diagrams for Copper at 25 to 300°C. *J. Electrochem. Soc.* **1997**, *144*, 3476.

(55) Kilcoyne, A. L. D.; Tyliszczak, T.; Steele, W. F.; Fakra, S.; Hitchcock, P.; Franck, K.; Anderson, E.; Harteneck, B.; Rightor, E. G.; Mitchell, G. E.; Hitchcock, A. P.; et al. Interferometer-Controlled Scanning Transmission X-Ray Microscopes at the Advanced Light Source. *J. Synchrotron Radiat.* **2003**, *10*, 125−136.

(56) Kaznatcheev, K. V.; Karunakaran, C.; Lanke, U. D.; Urquhart, S. G.; Obst, M.; Hitchcock, A. P. Soft X-ray spectromicroscopy beamline at the CLS: Commissioning results. *Nuclear Instruments and Methods in Physics Research Section A: Accelerators, Spectrometers, Detectors and Associated Equipment* **2007**, *582*, 96−99.

(57) Hitchcock, A. P.; Brion, C. E. Neon K-Shell Excitation Studied by Electron Energy-Loss Spectroscopy. *J. Phys. B: At. Mol. Phys.* **1980**, *13*, 3269−3273.

(58) Wang, J.; Botton, G. A.; West, M. M.; Hitchcock, A. P. Quantitative evaluation of radiation damage to polyethylene terephthalate by soft X-rays and high-energy electrons. *J. Phys. Chem. B* **2009**, *113*, 1869−1876.

(59) Zhang, W.; Melo, L. G. D. A.; Hitchcock, A. P.; Bassim, N. Electron beam damage of epoxy resin films studied by scanning transmission X-ray spectromicroscopy. *Micron* **2019**, *120*, 74−79.

(60) Melo, L. G.; Hitchcock, A. P. Electron beam damage of perfluorosulfonic acid studied by soft X-ray spectromicroscopy. *Micron* **2019**, *121*, 8−20.

(61) Martens, I.; Melo, L. G.; West, M. M.; Wilkinson, D. P.; Bizzotto, D.; Hitchcock, A. P. Imaging reactivity of the Pt−ionomer interface in fuel-cell catalyst layers. *ACS Catal.* **2020**, *10*, 8285−8292.

(62) Wu, J.; Melo, L. G.; Zhu, X.; West, M. M.; Berejnov, V.; Susac, D.; Stumper, J.; Hitchcock, A. P. 4D imaging of polymer electrolyte membrane fuel cell catalyst layers by soft X-ray spectro-tomography. *J. Power Sources* **2018**, *381*, 72−83.

(63) Hitchcock, A. P. Analysis of X-ray Images and Spectra (aXis2000): a toolkit for the analysis of X-ray spectromicroscopy data. *J. Electron Spectrosc. Relat. Phenom.* **2023**, *266*, 147360.

(64) Koprinarov, I. N.; Hitchcock, A. P.; McCrory, C. T.; Childs, R. F. Quantitative Mapping of Structured Polymeric Systems Using Singular Value Decomposition Analysis of soft X-ray Images. *J. Phys. Chem. B* **2002**, *106*, 5358−5364.

(65) Zhang, C.; Eraky, H.; Tan, S.; Hitchcock, A.; Higgins, D. In-situ Studies of Copper-based CO2 Reduction Electrocatalysts by Scanning Transmission Soft X-ray Microscopy. 2023, 10.26434/chemrxiv-2023-g2rj1. *ChemRxiv* (https://chemrxiv.org/engage/chemrxiv/article-details/645bfe08fb40f6b3ee5d903e) (accessed May 12, 2023).